Fiber Bragg Grating-Based Garment For Monitoring Human Body Temperature

Xiujuan Wang
Tiangong University
Yaming Jiang
Tiangong University
Siyi Xu
Tiangong University
Xiaozhi Li (shelly_lixz@126.com)
Tiangong University
Hao Liu
Tiangong University

Research Article

Keywords:

Posted Date: March 8th, 2022

DOI: https://doi.org/10.21203/rs.3.rs-1355756/v1

Abstract

Body temperature provides an insight into the physiological state of a person and body temperature changes reflect much information about human health. In the present study, a garment for monitoring human body temperature based on fiber Bragg grating (FBG) sensors is reported. The FBG sensor was encapsulated by a PMMA tube and calibrated in the thermostatic water bath. It has good vibration resistance and the wavelength changes about 0-1pm at 0.5-80Hz vibration frequency. The path of optical fiber was discussed and its bending radius was equal or greater than 20mm, so that the lower bending loss can be achieved when the garment was stretched on the human body. The FBG sensor, the optical fiber and garment were integrated together using hot melt glue by the electric iron and the hot press machine. Through experiments of monitoring human body temperature, the sensor can reach the human armpit temperature in about 15min with the upper arm close to the torso. For it is immune to electromagnetic interferences, the smart garment can be used in some special environments such as ultrasonography, magnetic resonance (MR) and aerospace.

Introduction

Body temperature is regarded as the first vital sign[1]. In daily life, it provides an insight into the physiological condition of a person. Either an elevated body temperature or a degraded body temperature indicates that the person is suffering from diseases. In medical area, continuous monitoring of body temperature can offer various kinds of information valuable for clinical diagnosis and as a useful guide to take suitable action[2]. Wearable flexible temperature sensors have been developing for monitoring body temperature[3, 4]. They measure the temperature by the electrical signal changes of the thermosensitive materials which are caused by the temperature change. Electrical signal is easily affected by electromagnetic, so the sensors can't be used in some special environments such as ultrasonography, magnetic resonance (MR) and aerospace.

Fiber Bragg Grating (FBG) sensors are sensitive to environmental variables, such as temperature, stress, bending and pressure. They have been widely applied in the fields of civil engineering, the automotive industry, aerospace, oil and gas industry and biomedicine as high-precision sensors[5–8].

Compared with electrical and mechanical sensors, they are immune to electromagnetic interferences. These features make FBG sensors more an emerging solution for the monitoring of physiological parameters, and they are particularly attractive for application in smart textiles. During the last decade, the garment, wearable straps, adhesive tape or insoles which were embedded the FBG sensors were used to monitoring body physiological parameters such as heart rate[9–11], body surface strain[12, 13], blood pressure [14, 15], respiration [9, 10, 16, 17], ballistocardiographic (BCG) signal [18], joint postures[19–22], plantar pressure[23–27] and temperature[28, 29]. As reported in reviews [29], the garment was divided into several blocks, the FBG temperature sensor was woven into the block and then the blocks were sewn together. The weaving process was complicated, and when the blocks were sewn together, the sensor may be

damaged. In addition, the report did not discuss how to integrate optical fiber, which is important for smart garment.

In this article, a FBG-based smart garment was developed for monitoring the body temperature. The principle, fabrication and encapsulation of FBG temperature sensor are presented in detail, and the sensor was calibrated and its performance tested. Then a new method of integrating garment, sensor and the path of optical fiber was designed and the integrated garment was worn on the body for temperature monitoring experiment. It aimed to provide a temperature monitoring solution for human body in electromagnetic environment.

The Principle Of Fbg Sensor

The advent of optical fiber with ultralow transmission loss has enabled optical communication to develop rapidly. It consists of a core, cladding and coating as shown in Fig. 1(a). While core and cladding are responsible for light guiding, the coating protects the fiber from external influence. Basically, the refractive index of the core by doping with germanium is slightly higher than that of the cladding, and light transmission obeys the principle of total internal reflection at the interface of core and cladding (Fig. 1(b)).

Germanium dopant also introduces photosensitivity to the optical fiber core which enables Bragg gratings to be inscribed on it. The refractive index of photosensitive fiber core is periodically modulated by Bragg gratings[30,31]. When a broadband light is launched through the core of the optical fiber with Bragg gratings, selective reflection of one particular narrow band of wavelengths, whose peak is termed as Bragg wavelength or central wavelength (Fig. 1(c)), is observed.

The Bragg wavelength is given by[32]

$$\lambda_B = 2\mathrm{n}_{eff}\Lambda$$

1

Where λ_B is the Bragg wavelength reflected by the Bragg grating, n_{eff} is the effective refractive index of the fiber and Λ is the grating period. FBGs are sensitive to external perturbations such as strain and temperature. When the strain or temperature near the grating changes, the effective refractive index or/and grating period get changed which lead to shift in reflected Bragg wavelength. The Bragg wavelength shift can be expressed by[32]

$$\frac{\Delta\lambda_B}{\lambda_B} = (1 - \mathrm{p}_{eff})\Delta\epsilon + (\alpha + \beta)\Delta\mathrm{T}$$

2

Where λ_B and $\Delta\lambda_B$ is initial Bragg wavelength and its change, Δε and ΔT are the stain and temperature change. P_{eff}, α and β are the photo-elastic coefficient, thermal expansion coefficient, and thermal-optic coefficient of fiber, respectively. The property of Bragg wavelength shift with respect to external strain or temperature is exploited for its sensing applications[32, 33].

In case the temperature of the external environment is constant, the ΔT = 0 and the equation of (2) is as follows

$$\frac{\Delta \lambda_B}{\lambda_B} = (1 - p_{eff})\Delta\epsilon$$

3

In case FBG is not affected by strain, Δε = 0 and Eq. (2) is as follows

$$\frac{\Delta \lambda_B}{\lambda_B} = (\alpha + \beta)\Delta T$$

4

Fbg Temperature Sensor Fabrication

FBG temperature sensor design and encapsulation. The relationship between the change of Bragg wavelength and temperature at constant strain is linear based on Eq. (4). The temperature sensitivity of bare FBG is about 10 pm/°C at about 1,550 nm in central wavelength[29] and the accuracy is about 0.1°C which basically cab meet the needs of human body temperature measurement. In order to prevent any posture of the human body from causing strain sensing to the FBG when the sensor is worn on the human body, the sensor can be encapsulated in a hard object. At the same time, the sensor should not affect the comfort of the garment. Stainless steel, ceramic and polymer materials are commonly used to encapsulate FBG. Stainless steel and ceramics have an excellent bending resistance and high temperature resistance, but stainless steel may cause discomfort when worn on the human body and ceramics are brittle and easily damaged. Polymethyl methacrylate (PMMA), known as plexiglass, has the bending strength of 110Mpa and the thermal deformation temperature of 74–107°C. Compared with stainless steel, it is safer and more comfortable when it is worn on the body. By comparing the shapes, commercial PMMA tube with 2mm outer diameter and 1.1mm inner diameter was chosen and two structures was designed to encapsulate FBGs as shown in Fig. 2. The single end of the optical fiber is adhered to the PMMA tube with the other end free in Fig. 2(a) and the two ends of the optical fiber are adhered to the ends of the PMMA tube respectively in Fig. 2(b).

In this study, a standard single mode optical fiber (Corning, SMF-28) was used for FBG fabrication. The fiber was loaded with hydrogen to render it photosensitive and striped off the acrylate coating of a small portion (about 10 mm), then a FBG of about 5 mm length was imprinted in the fiber core using the

standard phase mask technique and recoat with acrylic. The PMMA tube of 12mm length was used as the single-ended encapsulated tube and 15mm length as the duel-ended encapsulated tube. The optical fibers were covered with the ethylene-tetrafluoroethylene (ETFE) fluoropolymer as the protective jacket which could make the optical fiber more flexible and stronger. The optical fiber, jacket and the ends of the tubes were fixed with epoxy glue.

Calibration experiment of Sensor. Sensors should be calibrated against a certified thermometer prior to ingestion before prior to use. Currently, there is no consensus on the best approach for FBG sensors' calibration [34]. Some literatures reported calibrations by immersing FBG sensors into a thermostatic water bath [35] or different temperature liquid (liquid nitrogen (-195.8°C), ice slush (0°C), and boiling water (100°C)) with a platinum thermoresistance (Pt-100) element [36]. The calibration error of the former is related to the temperature accuracy of the water bath. The latter only calibrated three fixed-point, which directly affected the calibration accuracy.

In this work, the block diagram of the experimental setup is depicted in Fig. 3(a). The thermostatic water bath was heated to different discrete temperatures. A platinum resistance thermometer (YET-720L, Kaipusen) with a reported accuracy of ± 0.1°C and a Pt-100 platinum resistance temperature sensor were used as the standard measure of water bath temperature. The FBG sensor and the Pt-100 sensor were immersed in the same place of the water bath. At each discrete temperature, the values of thermometer and FBG wavelength were recorded when they fluctuated about 30 seconds slightly around a fixed value. Three calibration experiments were carried out three times at different times.

Figure 3(b) and Fig. 3(c) show the relationship between wavelength and temperature of single-ended FBG sensor and dual-ended FBG sensor respectively. For the single-ended FBG sensor, it can be observed that the wavelength of Bragg grating increases with temperature and the wavelength shifts of all three trial runs agree well with each other which shows the sensors has a good stability and repeatability. However, for the dual-ended FBG sensor, the wavelength of the Bragg grating increases with temperature, but the wavelength shifts of all three experiments are not quite consistent. This may be caused by the change in the length of the PMMA tube (the coefficient of linear expansion is approximately $(5 \sim 9)*10^{-5}$/°C.) due to the change in temperature, which resulted in the strain applied to the FBG. So further experiments were carried out with single-ended FBG sensors.

The results of the three calibrations are respectively fitted with linear equations, and the calibration formula with the largest correlation coefficient is selected and it is expressed as follows:

$y = 99160.7522e\text{-}06*x\text{-}15367179893.6327e\text{-}05$ $R^2 = 0.9999$ (5)

The measured temperature response at a constant strain is nearly linear about 10.1 pm/∘C.

Anti-vibration performance test of FBG sensor. The human body is the source of vibration. The movement of the human body will cause the human body to vibrate, and even human body is at rest, the organs are

also in vibration. The range of frequencies considered by the ISO for health, comfort and perception is 0.5 Hz to 80 Hz [37].

When the FGB sensor is worn on the human body, the vibration of human body organs and movement will cause the vibration of the sensor. The article tested the impact of vibration on the sensor's sensing performance. The test setup is shown in Fig. 4(a). The FBG sensor was fixed on the vibrator by adhesive tape, and the function waveform generator was used to adjust the vibration frequency. The linear power amplifier converts the signal input from the function waveform generator into a stable and adjustable excitation current, which is fed to the vibrator. Under the action of the excitation current, the vibrator generates an excitation force to make it vibrate. By setting different vibration frequency from 0.5HZ to 80HZ, wavelength change of the FBG sensor was recorded. The experiment was carried out in a constant temperature and humidity laboratory which the temperature change is about ± 0.5°C. The result in Fig. 4(b) shows that the wavelength of the sensor changed about 0-1pm at any vibration frequency.

Temperature calibration verification. The result of FBG sensor calibration was verified by two methods. One was static temperature measurement, the other was dynamic body temperature monitoring. The calibration formula (5) was input the software by programming which was used to convert the wavelength to temperature. At the room temperature about 22°C, the water bath was heated to 25, 30, 35, 40, 45, 50, 55, 60°C. At every discrete temperature, the FBG sensor and the Pt-100 sensor were immersed in the same place. The temperature values of pt100 and FBG sensor were recorded when they were stable. Figure 5(a) and Fig. 5(b) show the values of FBG sensor and pt-100 sensor and the error of FBG sensor relative to pt-100 sensor, and the absolute values of the errors are all less than 0.2°C. Then at the room temperature about 25°C, the Pt-100 sensor and FBG sensor were placed in the armpit of the subject at same time and the sensors were clamped by the arm. After about 30 minutes, the sensors were removed from armpit. The platinum resistance thermometer recorded one data per second, and the FBG interrogator recorded 10 data per second. By calculating the average value of the data recorded by the FBG interrogator per second, the temperature monitored by the two sensors is shown in Fig. 5(c) and the response time of pt-100 sensor and FBG sensor are 19s and 3s as shown in insets of Fig. 5(c). Figure 5(d) shows the errors of FBG sensor relative to pt-100 sensor when they were stable, and the absolute values of the errors are also less than 0.2°C. The error of FBG sensor mainly came from human body vibration, calibration formula and the accuracy of the platinum resistance thermometer.

Integration Of Sensor And Garment

Integration design. The mouth, axillary and rectal thermometry are the common methods of human body temperature measurement in the medical field, of which the axillary thermometry is the most convenient. The skin surface of the human armpit is relatively flat, and the sensor can fully contact the human skin at this position.

In this work, the elastic tight-fitting inner vest was chosen as the FBG sensor carrier which made the sensor easier and comfortable to wear on the human body. There are many inner vest in different fabrics

and styles on the market. Sleeveless inner vest which was made of the rib knitted fabric consisting of cotton and spandex was chosen. The integrated solution of inner vest and FBG sensor was designed based on the axillary thermometry as shown in Fig. 6. The FBG sensor was placed at the armhole's lowest part of the inner vest (Fig. 6(a)), which is also the closest part to the armpit when the vest is worn on the body. Optical fiber which is used to transmit signals is also important for the integration of the entire garment. If it is free, it may affect signal transmission or pulled off. For the tight garment is worn on the human body, it may be stretched horizontally or vertically. When the optical fiber is integrated into the garment in a straight line, it is easily damaged as the garment is stretched. Therefore, the path of optical fiber was designed as a curved line, as shown in Fig. 6(b). When the garment is stretched, the curvature of the optical fiber path changes which can protect the optical fiber from being broken. The heat press machine was employed to glue the FBG sensor and optical fiber on inner vest by the hot melt glue as Fig. 6(c) is shown. Since the thermal deformation temperature of PMMA is about 68–69°C, the FBG sensor was carefully glued to the vest with an electric iron in order to avoid damage to the PMMA tube.

Optimizing the path of optical fiber. As Fig. 7(a) is shown, the bending of optical fiber modifies the guiding properties of optical fiber and cannot meet the total reflection condition, resulting in an increase of its radiative (outpropagating) part and the loss of optical power which affects FBG sensing performance. Different math models[38–41] have been suggested to calculate the relationship between the bending loss and radius of curvature. The parameters such as refractive index, wavelength and their variations under various experimental conditions (temperature) can affect the loss results, so almost every theoretical model is disagreement with the real experimental results. However, all theoretical models have the same conclusion, that is, the bending loss increases as the radius decreases, and as the number of wrapping turns increases within a certain bending radius. When the bending radius is smaller than the threshold value, the oscillation of bending loss appears[41, 42].

In this work, bending loss of optical fiber was tested and the schematic diagram of the set-up is shown in Fig. 7(b) and Fig. 7(e). The two ends of the optical fiber were respectively connected to the optical laser source (λ = 1550) and the optical power meter. For bending the fiber, wooden cylindrical rod with different radius (R = 22.5, 20, 17.5, 15, 12.5, 10, 7.5, 6, 5, 4, 2.5mm) was employed. The influence of bending radius (R) on loss was investigated at first. The result in Fig. 7(c) shows the bending loss gets bigger and increases exponentially as the bending radius (R) is less than 10mm. Then the influence of wrapping turn number (N) on loss was tested using the cylindrical rods with the radius $R \geq 10$mm and up to 15 turns were investigated. As shown in Fig. 7(d), the bending radius R = 10mm is the critical bending radius, and with the bending radius R > 10 mm, the bending loss effect is small.

The path of optical fiber was designed as the curved line in Fig. 7(e). So the article also tested the bending loss of the path's bending number (N). The path was printed on the paper along which the optical fiber was gradually pasted. The result shown in Fig. 7(f) is consistent with the loss of wrapping turn.

The paper tested the AD value of the center wavelength after being bent 5 times. (1) Initial wavelength without bending. (2) When the bending radius is 7.5mm, the central wavelength AD value. (3) The

bending radius is 10mm, and the center wavelength is AD value. (4) When the bending radius is 12.5mm, the central wavelength AD value.

The paper tested the AD (analog-to-digital) value of the FBG reflected wavelength after the fiber was bent 5 times. AD refers to the output value of the light intensity detected by the spectrophotometer through the analog-to-digital converter, the larger the value, the easier it is to detect the center wavelength. As shown in Fig. 8, when the bending radius is 7.5mm and 10mm, the AD value fluctuates greatly. When the bending radius is 12.5mm, the AD value wavelength is smaller.

From the above results, the bending radius(R) of the optical fiber must be bigger than 10mm under various stretching conditions.

The bending radius gets bigger with the garment stretched in vertical direction, and becomes smaller with the garment stretched in horizontal direction. Therefore, the change of bending radius with the optical fiber stretched in horizontal direction is very important to design its path. When the garment is worn, the movement of the body causes the garment to stretch horizontally. As Fig. 9(a) is shown, the maximum horizontal stretch rate of garment caused by human breathing is 12%-14% and caused by the bending of the torso is 16%-18%. Four paths with different bending radius were designed. The fabric was manually stretched to different rates as Fig. 9(c) is shown. The stretched rate and the bending radius of optical fiber were calculated by digital image processing technology. The bending radius decreased with the increase of the stretch rate as shown in Fig. 9(b) and for an optical fiber with an initial bending radius $R \geq 20$mm, the bend radius was still greater than 10mm after being stretched 25%. In fact, when the appropriate size of the vest is worn on the body, it could not be stretched so much and the bending radius is bigger than this method. According to the above conclusions, bending radius of the optical fiber path is designed to be greater than 20mm. In fact, the optical fiber was pasted on the vest by the hot melt glue which made the bonding part more difficult to stretch than other part. So when the appropriate size of the vest is worn on the body, stretch rate of optical fiber path will be smaller than manual stretching. From these results, bending radius of the optical fiber path is designed to be equal or greater than 20mm.

Body temperature monitoring test. According to the above conclusions, the FBG sensor and the optical fiber with bending radius 20mm was fixed to the vest with a needle and thread, and then they were integrated together using the electric iron and the hot press machine as shown in Fig. 10(a).

At the room temperature about 23°C, the subject put on the inner vest, a long-sleeved T-shirt and a coat in order and the sensor was connected with the FBG interrogator. Then Pt-100 sensor was stuck in the armpit using adhesive tape to keep it from slipping. The arm was close to the torso reduce underarm air exchange.

The temperature monitoring curves of FBG sensor and pt-100 sensor are shown in Fig. 10(b). The pt-100 sensor was placed under the human armpit and began to change steadily after about 25s. The FBG sensors was affected by the microclimate inside the garment and began to change steadily after about 10min. After about 15min, the temperature values of the two sensors were essentially coincident.

Figure 10(c) shows the error of FBG sensor relative to pt-100 sensor and the absolute values are all less than 0.2°C. Figure 10(d) and Fig. 10(e) show that the temperature values of the FBG sensor and the PT-100 sensor changed the same when the arm swung, and these indicate that the FBG sensor was not affected by strain.

Conclusion

This paper demonstrates the principle and application of FGB sensing technology to design and develop an inner vest for monitoring human body temperature. The FBG sensor was ergonomically designed. It was encapsulated, calibrated and tested the anti-vibration performance in the laboratory. It was placed at the armhole's lowest part of the inner vest. The design of the optical fiber path was analyzed in great detail. Through multiple tests, the inner vest integrated with the FBG sensor is very convenient for monitoring human body temperature. The FBG sensor is waterproof for its encapsulation, so it can be washed with right washing method.

Compared to electronic sensors, FBG sensors are immune to electromagnetic interference, so the inner vest can be used to monitor the patient's temperature during MR or ultrasound, as well as the pilot's temperature. As electromagnetic environment of modern is becoming complex, its application will become more and more extensive.

Data Availability

The datasets used and/or analysed during the current study are available from the corresponding author on reasonable request.

Declarations

Statements

All experimental protocols were approved by the Tiangong University. The research were carried out in accordance with the Declaration of Helsinki and relevant guidelines and regulations and have obtained informed consent from all participants.

Competing interests

All authors declare no competing interests.

Acknowledgements

The research is supported by the National Key Research and Development Program of China (grant no. 2019YFF0302100) and the National Natural Science Foundation of China (grant no. 51473122).

Author contributions

X.Z.L. and H.L. conceived the idea. X.J.W. and X.Z.L. implemented the concept. Experimental works were carried out by X.J.W., X.Z.L. and S.Y. and Y.M.J. took part in the analysis and discussion. X.J.W., X.Z.L. and H.L. drafted the paper. All authors contributed to the writing.

References

1. Khan Y., Ostfeld A.E., Lochner C.M., Pierre A. and Arias A.C. Monitoring of Vital Signs with Flexible and Wearable Medical Devices. Adv. Mater., **28**, 4373–4395 (2016).
2. Husain MD, Naqvi S, Atalay O. Measuring Human Body Temperature through Temperature Sensing Fabric. AATCC J. Res., **3**, 1–12 (2016).
3. Su Y. et al. Printable, Highly Sensitive Flexible Temperature Sensors for Human Body Temperature Monitoring A Review. Nanoscale Res. Lett., **15**, 200 (2020).
4. Hughes-Riley T., Jobling P., Dias T. and Faulkner S.H. An investigation of temperature-sensing textiles for temperature monitoring during sub-maximal cycling trials. Text. Res. J., **91**, 624–645 (2021).
5. Krebber K. Smart technical textiles based on fiber optic sensors. *In Current Developments in Optical Fiber Technology*, https://www.intechopen.com/chapters/45075 (2013).
6. Carlo M., Paola S. and Emiliano S. Medical smart textiles based on fiber optic technology: An overview. J. of Funct. Biomater., **6**, 204–221 (2015).
7. Liu Z.Y., Zhang Z.F., Tam W.Y. and Tao X.M. Multifunctional Smart Optical Fibers: Materials. Fabrication, and Sensing Applications. Photonics, **6**, 48; http://dx.doi.org/10.3390/photonics6020048 (2019).
8. Roriz P., Silva S., Frazao O. and Novais S. Optical Fiber Temperature Sensors and Their Biomedical Applications. Sensors, **20**, 2113; http://dx.doi.org/10.3390/s20072113 (2020).
9. Dziuda L., Skibniewski F.W., Krej M. and Lewandowski J. Monitoring Respiration and Cardiac Activity Using Fiber Bragg Grating-Based Sensor. IEEE T. Bio.-Med. Eng., **59**, 1934–1941 (2012).
10. Dziuda L., Skibniewski F.W., Krej M. and Baran P.M. Fiber Bragg grating-based sensor for monitoring respiration and heart activity during magnetic resonance imaging examinations. J. Biomed. Opt., **18**, 057006; http://dx.doi.org/ 10.1117/1.JBO.18.5.057006 (2013).
11. Fajkus M. et al. Fiber optic sensor encapsulated in polydimethylsiloxane for heart rate monitoring. *Proc. of SPIE*, **10208**, 102080W; https://doi.org/10.1117/12.2256718 (2017).
12. Subbarao G.P.A., Narasipur O.S., Kalegowda A. and Asokan S. A novel fiber Bragg grating based sensing methodology for direct measurement of surface strain on body muscles during physical exercises. Int. J. Optomechatronic, **6**, 189–198 (2012).
13. Lee S.B., Jung Y.J., Choi H.K., Sohn I.B. and Lee J.H. Hybrid LPG-FBG based high-resolution micro bending strain sensor. Sensors, **21**, 22; https://dx.doi.org/ 10.3390/s21010022 (2020).
14. Katsuragawa Y. and Ishizawa H. Non-invasive blood pressure measurement by pulse wave analysis using FBG sensor. In Pro. Of *I2MTC*, 511–515 (2015).

15. Kumar N.V. et al. Fiber Bragg grating-based pulse monitoring device for real-time non-invasive blood pressure measurement-a feasibility study. IEEE Sens. J., **21**, 9179–9185 (2021).
16. Witt J. et al. Medical textiles with embedded fiber optic sensors for monitoring of respiratory movement. IEEE Sens. J, **12**, 246–254 (2012).
17. Manujlo A. and Osuch T. Temperature fiber Bragg grating based sensor for respiration monitoring. *Proc. of SPIE*, **10445**, 104451A; http://doi.org/ 10.1109/I2MTC.2015.7151320 (2017).
18. Dziuda L. and Skibniewski F.W. A new approach to ballistocardiographic measurements using fibre Bragg grating-based sensors. Biocybern. Biomed. Eng., **34**, 101–116 (2014).
19. Umesh S., Padma S., Srinivas T. and Asokan S. Fiber Bragg grating goniometer for joint angle measurement. IEEE Sens. J., **18**, 216–222 (2018).
20. Abro Z.A. et al. A novel flex sensor-based flexible smart garment for monitoring body postures. J. Ind. Text., **49**, 262–274 (2019).
21. Abro Z.A. et al. A fiber Bragg grating-based smart wearable belt for monitoring knee joint postures. Text. Res. J., **90**, 386–394 (2019).
22. Hong C.Y., Abro Z.A., Zhang Y.F. and Lakho R.A. An FBG-based smart wearable ring fabricated using FDM for monitoring body joint motion. J. Ind. Text., **50**, 1660–1673 (2021).
23. Suresh R., Bhalla S., Hao J. and Singh C. Development of a high resolution plantar pressure monitoring pad based on fiber Bragg grating (FBG) sensors. Technol. Health Care, **23**, 785–794 (2015).
24. Liang T.C., Lin J.J. and Guo L.Y. Plantar Pressure Detection with Fiber Bragg Gratings Sensing System. Sensors, **16**, 1766; http://doi.org/ 10.3390/s16101766 (2016).
25. Vilarinho D. et al. POFBG-Embedded Cork Insole for Plantar Pressure Monitoring. Sensors, **17**, 2924, http://doi.org/ 10.3390/s17122924 (2017).
26. Leal A.G. et al. Fiber Bragg Based Sensors for Foot Plantar Pressure Analysis. Pro. Of BIOSTEC, **1024**, 3–25 (2019).
27. Lakho R.A., Zhang Y.F., Jiang J.H., Hong C.Y. and Abro Z.A. A smart insole for monitoring plantar pressure based on the fiber Bragg grating sensing technique. Text. Res. J., **89**, 3433–3446 (2019).
28. Ghosh S., Amidei C. and Furrow K. Development of a sensor-embedded flexible textile structure for apparel or large area applications. Indian J. Fibre Text., **30**, 42–48 (2005).
29. Li H.Q., Yang H.J., Li E.B., Liu Z.H. and Wang K.J. Wearable sensors in intelligent clothing for measuring human body temperature based on optical fiber Bragg grating. Opt. Express, **20**, 11740; https://doi.org/10.1364/OE.20.011740 (2012).
30. Hill K. O., Fujii Y., Johnson D. C. and Kawasaki B.S. Photosensitivity in optical fiber waveguides Application to reflection filter fabrication. Appl. Phys. Lett., **32**, 647–649 (1978).
31. Morey W. W., Meltz G. and W. H. Glenn. Fiber optic Bragg grating sensors. Pro. Of SPIE, **1169**, 98–107 (1990).

32. Othonos A and Kalli K. Fiber Bragg gratings: fundamentals and applications in telecommunications and sensing. Artech House Publishers: Boston, USA, 1–112 (1999).
33. Tahir B.A., Ali J. and Rahman R.A. Fabrication of fiber grating by phase mask and its sensing application. J. Optoelectron. Adv. M., **8**, 1604–1609 (2006).
34. Hunt A.P. and Stewart I.B. Calibration of an ingestible temperature sensor. Physiol. Meas., **29**, N71-N78 (2008).
35. Ma B. and Sun Y.C. Research on Real-Time Monitoring of Human Body Temperature Based on Fiber Bragg Grating Sensing Technology. Pro. Of ICCCS, **11064**, 124–133 (2018).
36. Samset E. et al. Temperature measurement in soft tissue using a distributed fibre Bragg-grating sensor system. Minim. Invasive Ther., **10**, 89–93 (2001).
37. ISO. ISO 2631-1–1997 Mechanical vibration and shock—Evaluation of human exposure to whole-body vibration—part 1: General requirement. *ISO*, 1–6 (1997).
38. Marcuse D. Curvature loss formula for optical fibers. J. Opt. Soc. Am., **66**, 216–220 (1976).
39. Faustini L. and Martini G. Bend loss in single-mode fibers. J. Lightwave Technol., **15**, 671–679 (1997).
40. Tsao S.L. and Cheng W.M. Simplified formula of bending loss for optical fiber sensors. Fiber Integrated Opt., **21**, 333–344 (2002).
41. Zendehnam A., Mirzaei M., Farashiani A. and Farahani L. H. Investigation of bending loss in a single-mode optical fibre. Pramana J. Phys., **74**, 591–603 (2010).
42. Renner H. Bending losses of coated single-mode fibers: a simple approach. J. Lightwave Technol., **10**, 544–551 (1992).

Figures

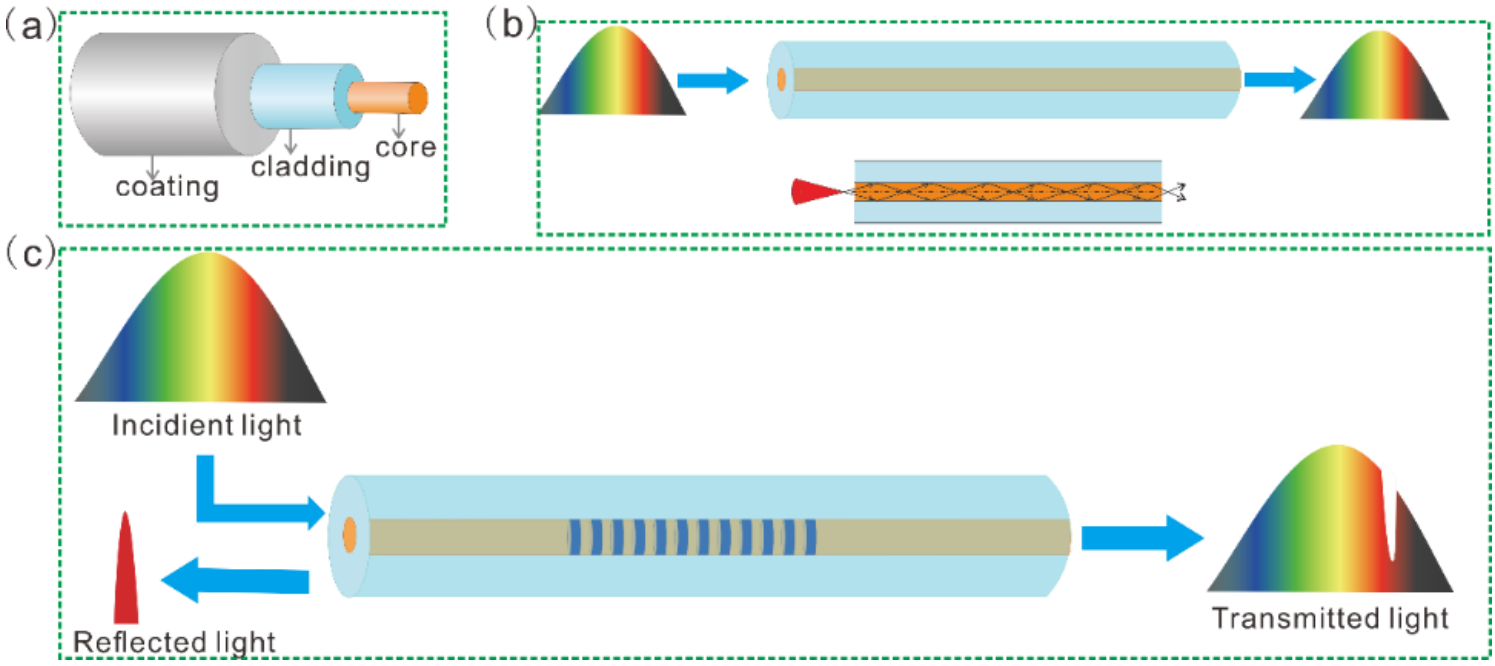

Figure 1

Working principle of Fiber Bragg grating (FBG)

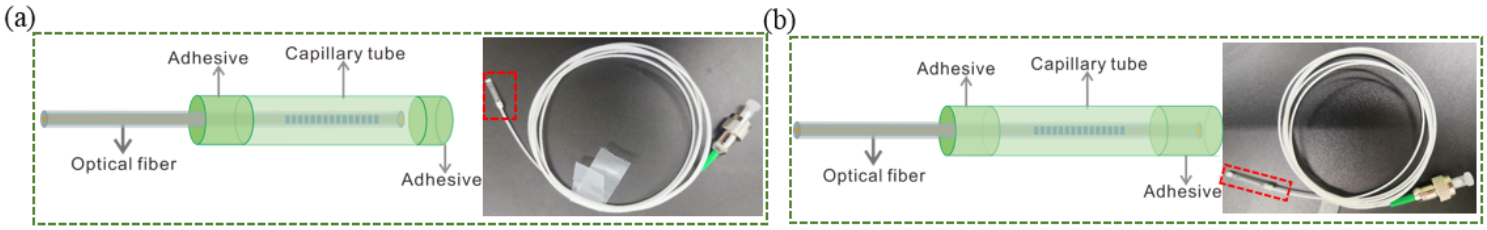

Figure 2

The structure of the sensors, (a) single-ended encapsulation and (b) dual-ended encapsulation.

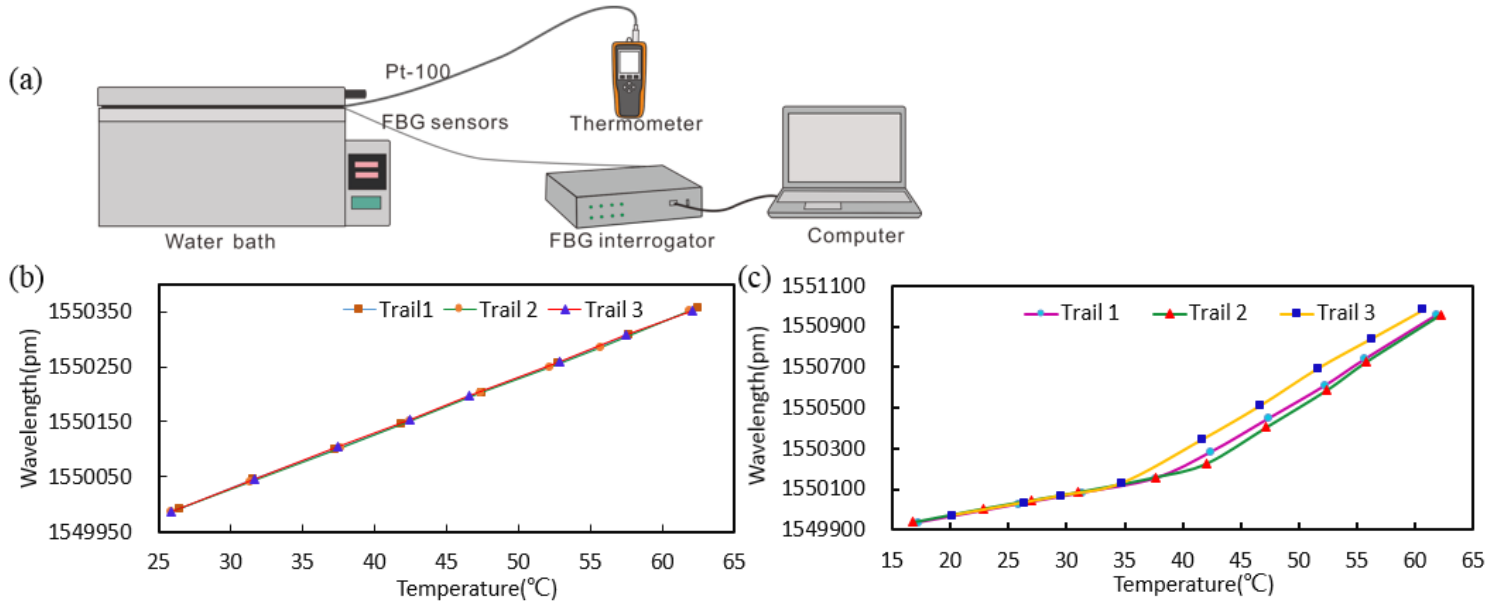

Figure 3

The calibration experiments. (a) The calibration experiment setup. (b) and (c) the relationship between wavelength and temperature of single-ended FBG sensor and dual-ended FBG sensor respectively.

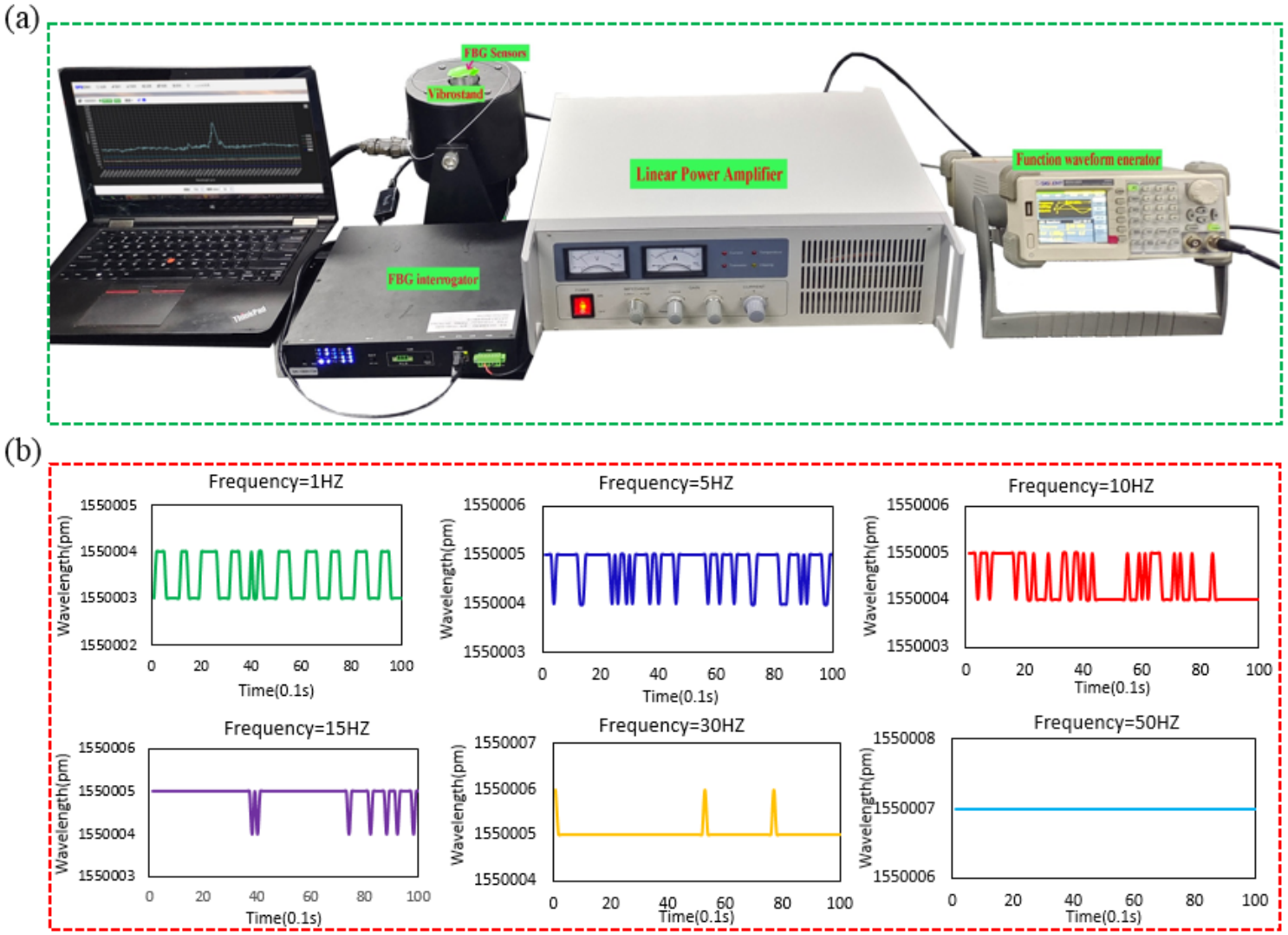

Figure 4

Anti-vibration performance test of FBG sensor, (a) the experiment setup, (b) the wavelength changes with different vibration frequencies

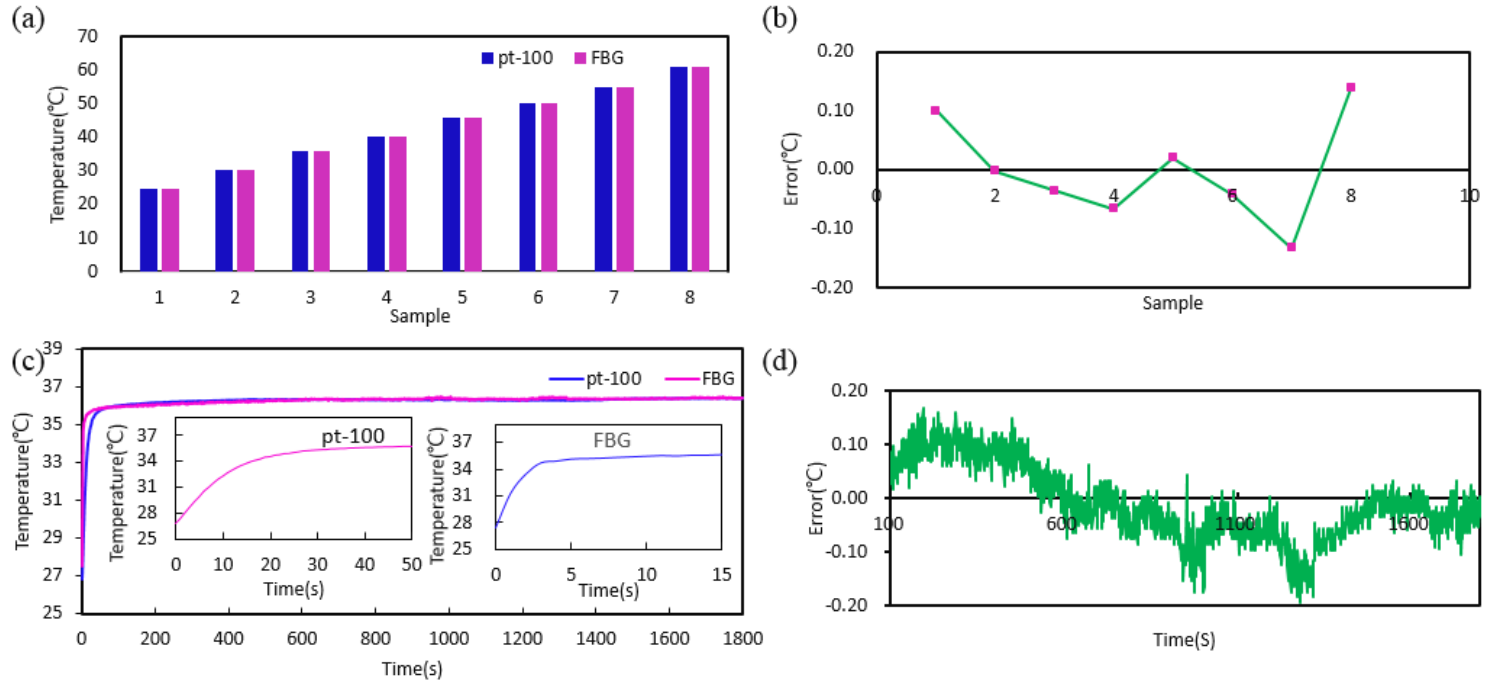

Figure 5

Temperature calibration verification and its error of FBG sensor. (a) The static temperature measurement by FBG sensor and pt-100 senor and (b)The errors of FBG sensor relative to pt-100 sensor. (c) The body temperature monitoring about 30min by FBG sensor and pt-100 senor and (d)The errors of FBG sensor relative to pt-100 sensor.

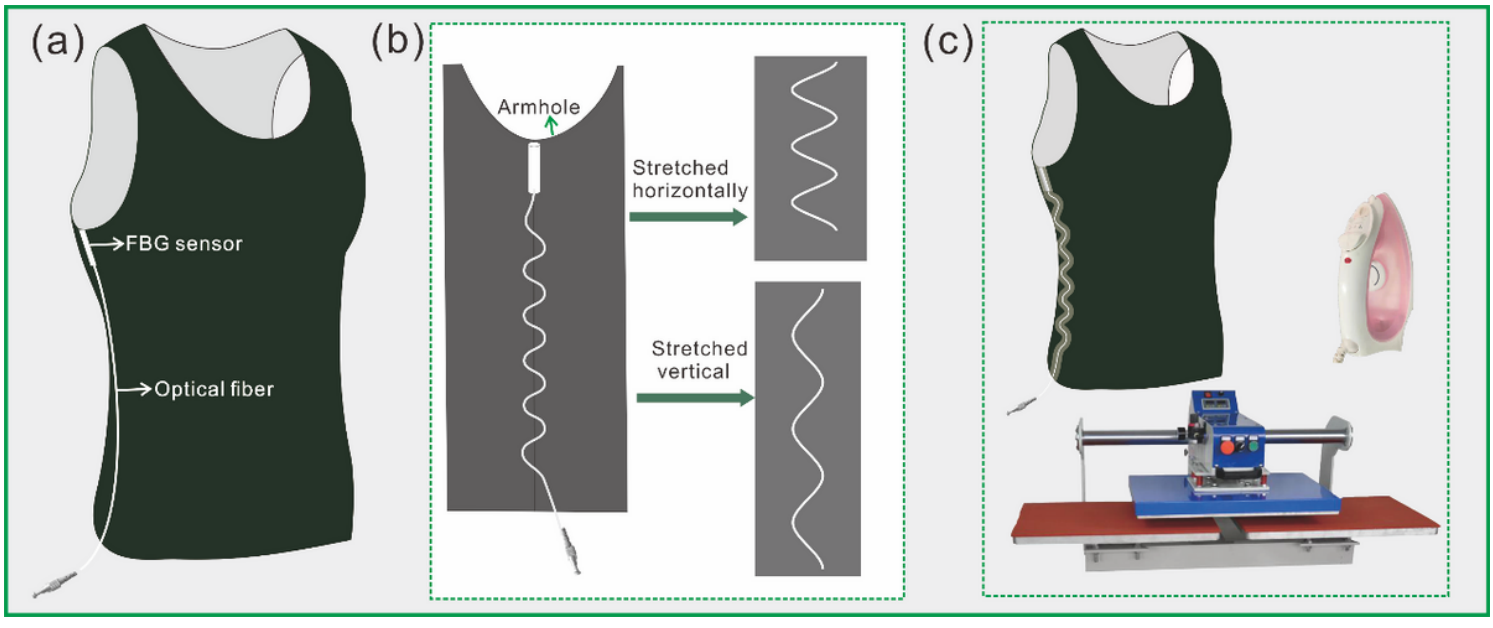

Figure 6

The integrated solution of garment and FBG sensor. (a) The position of FBG, (b) the path design of optical fiber, and (c) the method of the vest, the FBG sensor and optical fiber integration.

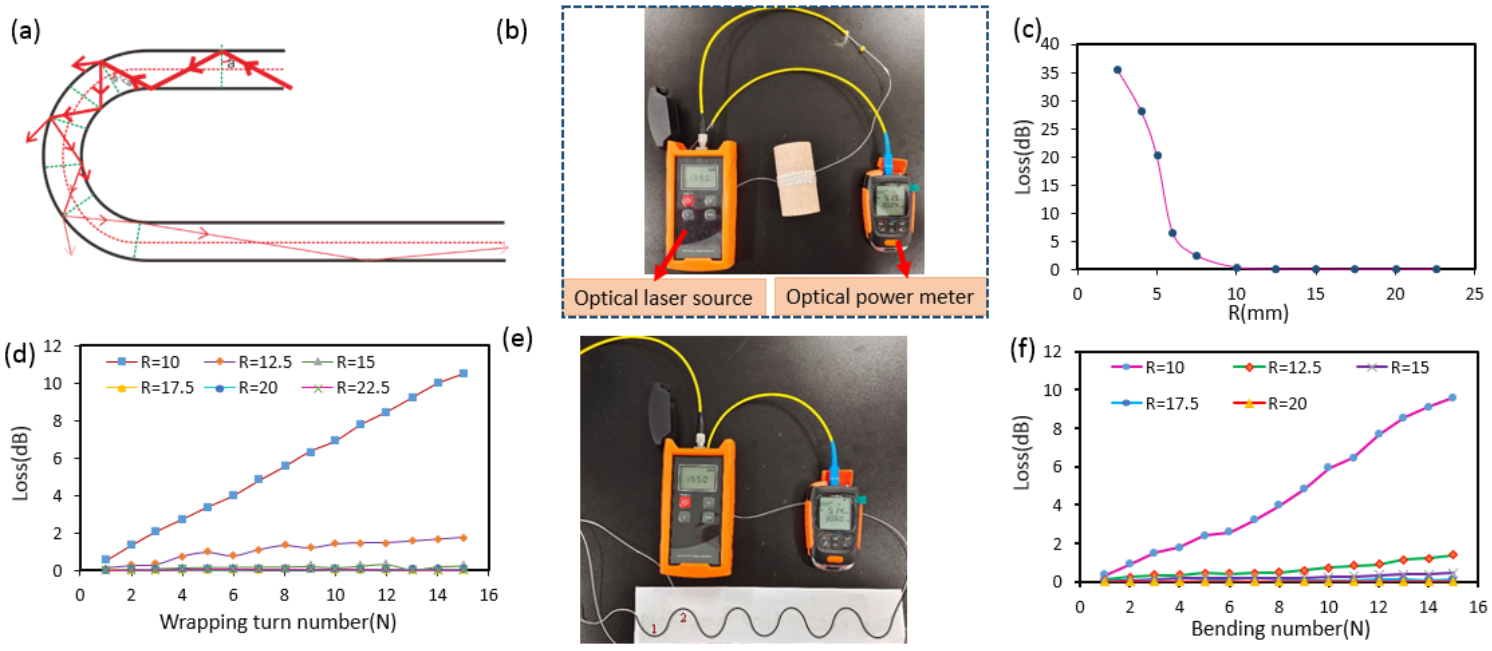

Figure 7

The bending loss test of optical fiber. (a) The light guiding properties when the optical fiber is bent. (b) Schematic diagram of the optical set-up for measuring loss of optical with different radiuses and wrapping turn numbers. (c) and (d) are the variation of loss against bending radius and wrapping turn number. (e) Schematic diagram of the optical set-up for measuring loss of optical with different curves. (f) Variation of loss against path bending number.

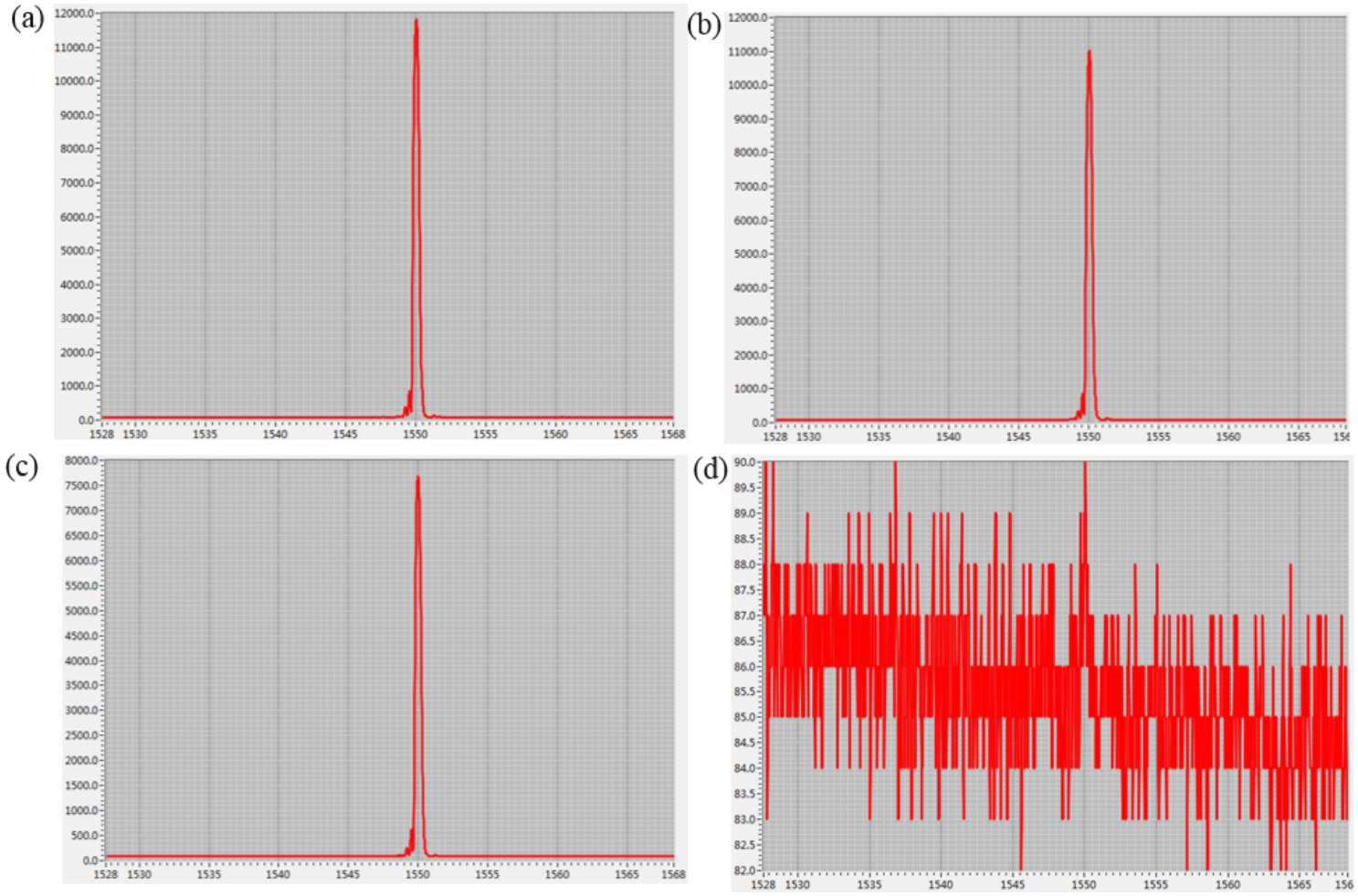

Figure 8

The relationship between fiber bending and AD value fluctuate of the FBG reflected wavelength. (a) Optical fiber almost no bend, (b) the bending radius with 12.5mm, (c) the bending radius with 10mm and (d) the bending radius with 7.5mm.

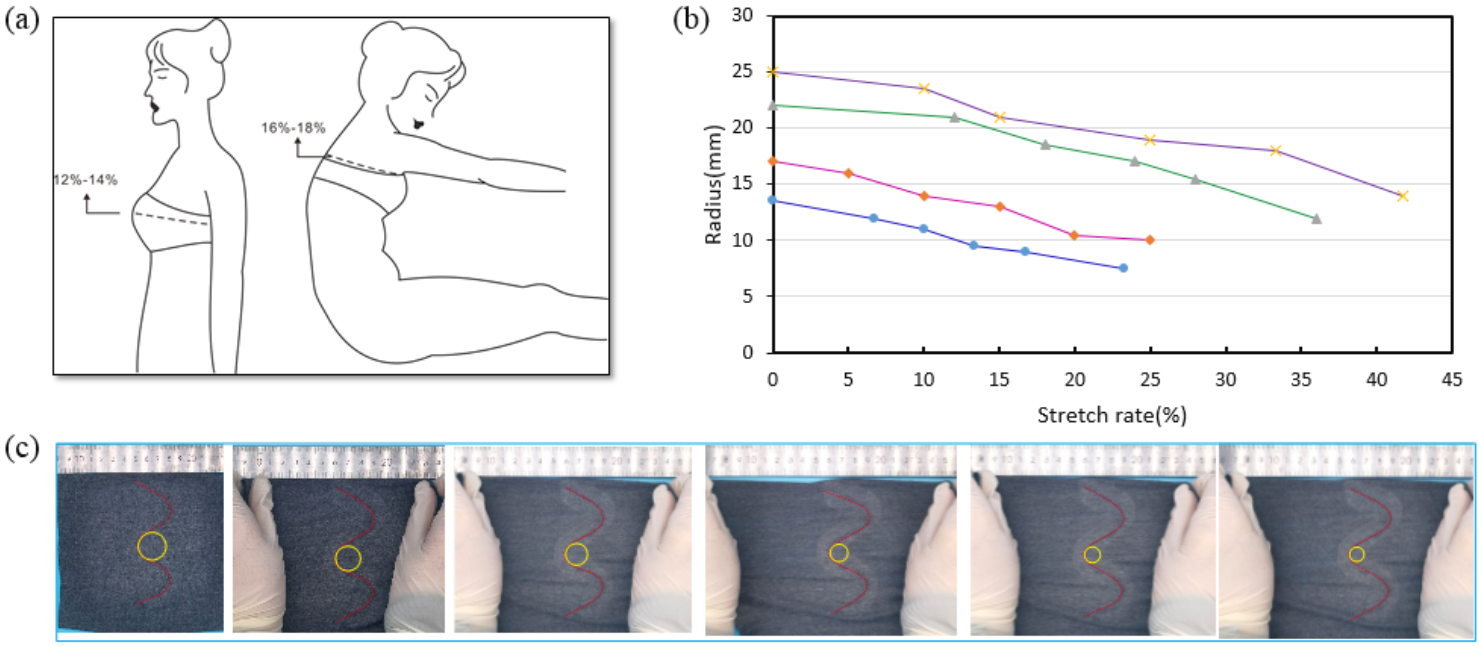

Figure 9

The relationship between the horizontal stretching of the optical fiber path and the bending radius. (a) The effect of human movement on the maximum horizontal stretch rate of garment. (b) The relationship between the bending radius and the stretch rate with different initial bending radius. (c) The manual stretching test of optical fiber path.

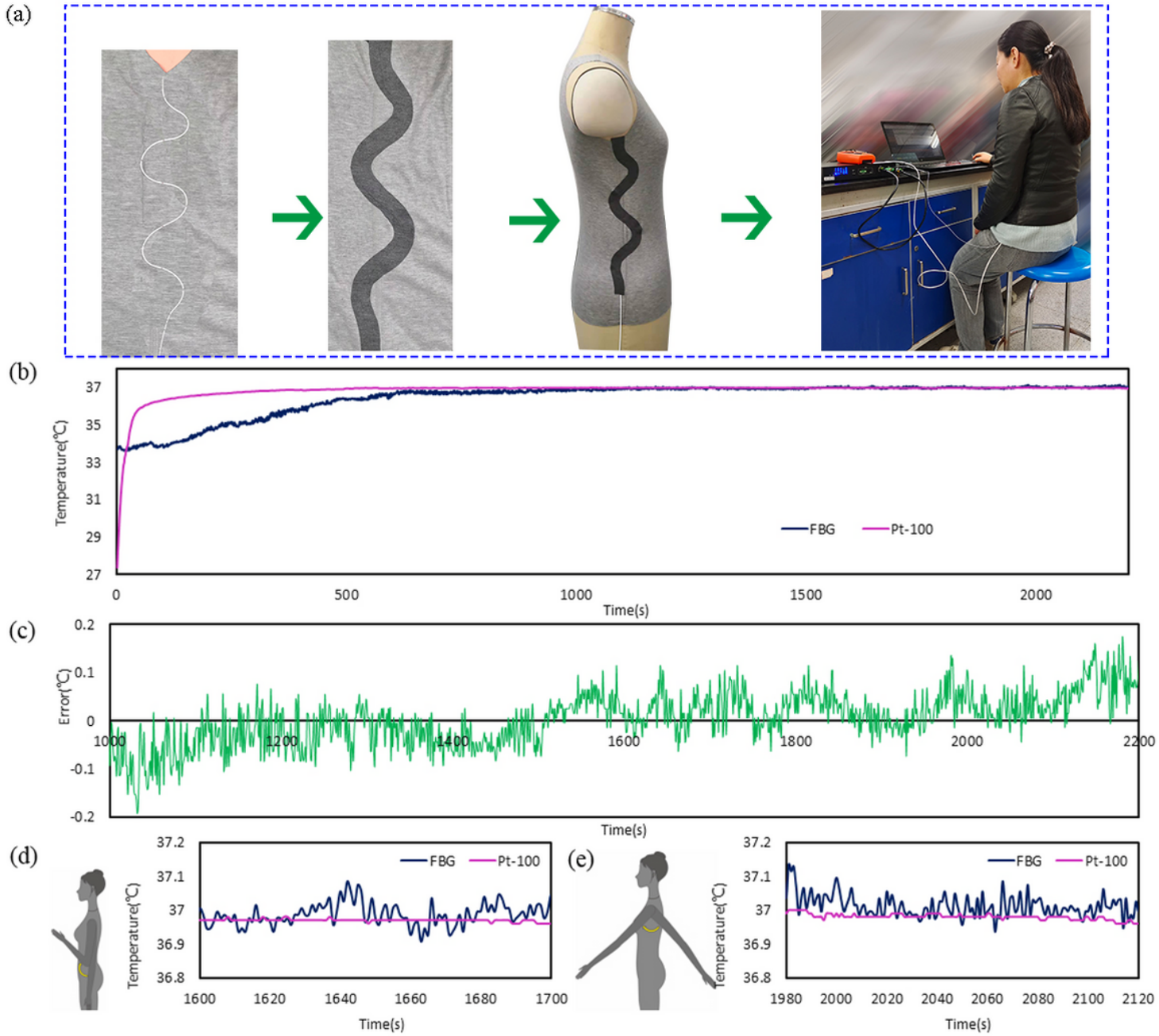

Figure 10

Body temperature monitoring test by worn on the inner vest. (a) The integration process of inner vest. (b) The body temperature monitoring curves of whole process. (c) The error of FBG sensor relative to pt-100 sensor. (d) and (e) the human body temperature when arm swing.

Supplementary Files

This is a list of supplementary files associated with this preprint. Click to download.

- Fig3calibrationexperiments.xlsx
- Fig4vibrationtest.xlsx
- Fig5bodytemperaturemonitoring.xlsx
- Fig5statictemperaturemeasurement.xlsx
- Fig7bendinglosstest.xlsx
- Fig9thehorizontalstretchingtest.xlsx
- Fig10.xlsx